ACADEMIC
PRESS

Independent component analysis of nondeterministic fMRI signal sources

Vesa Kiviniemi,[a],* Juha-Heikki Kantola,[a] Jukka Jauhiainen,[b]
Aapo Hyvärinen,[c] and Osmo Tervonen[a]

[a] Department of Diagnostic Radiology, University of Oulu, Oulu, Finland
[b] Oulu Polytechnic, Institute of Technology, Oulu, Finland
[c] Neural Networks Research Center, Helsinki University of Technology, Helsinki, Finland

Abstract

Neuronal activation can be separated from other signal sources of functional magnetic resonance imaging (fMRI) data by using independent component analysis (ICA). Without deliberate neuronal activity of the brain cortex, the fMRI signal is a stochastic sum of various physiological and artifact related signal sources. The ability of spatial-domain ICA to separate spontaneous physiological signal sources was evaluated in 15 anesthetized children known to present prominent vasomotor fluctuations in the functional cortices. ICA separated multiple clustered signal sources in the primary sensory areas in all of the subjects. The spatial distribution and frequency spectra of the signal sources correspond to the known properties of 0.03-Hz very-low-frequency vasomotor waves in fMRI data. In addition, ICA was able to separate major artery and sagittal sinus related signal sources in each subject. The characteristics of the blood vessel related signal sources were different from the parenchyma sources. ICA analysis of fMRI can be used for both assessing the statistical independence of brain signals and segmenting nondeterministic signal sources for further analysis.
© 2003 Elsevier Science (USA). All rights reserved.

Keywords: fMRI; ICA; Child; Anesthesia; Vasomotor fluctuation

Introduction

Controlled neuronal activation of the brain functional cortex produces signal enhancement that can be detected with functional magnetic resonance imaging (fMRI) (Ogawa et al., 1990, 1998). Without deliberate neuronal activity the T2*-weighted fMRI time domain signal is influenced by uncontrolled, non-Gaussian signal sources including spontaneous neuronal activity, vasomotor fluctuations, and thermal, instrumentational, and other noise sources (Weisskoff et al., 1996; Mitra et al., 1997; Frank et al., 2001). In the past, most of the low-frequency signal sources have been regarded as nuisances that obscure fMRI results and focus has been in attenuating their effects. Recently, however, spontaneous activity of connected neural networks has been related to fMRI signal fluctuations at frequencies lower than 0.1 Hz (Biswal et al., 1995; Li et al., 1999; Cordes et al., 2000). In anesthesia, the fMRI signal of primary functional cortices is dominated by 0.03-Hz signal intensity fluctuation that closely resembles spontaneous vasomotor (or Mayer) waves (Kiviniemi et al., 2000; Kleinfeld et al., 1998; Obrig et al., 2000).

Analysis methods suited for controlled activity, i.e., methods that can utilize a priori assumptions about the spatial distributions and temporal waveforms of the fMRI signal sources, may not be completely accurate in characterizing the uncontrolled physiological signal sources. More robust analysis of nondeterministic or stochastic processes, like vasomotor waves, is based on the statistical analysis of the measured signal (Oppenheim et al., 1996). Independent component analysis (ICA) has recently been shown to be

able to separate activation, physiological, and other signal sources in fMRI studies (McKeown et al., 1998; McKeown and Sejnowski, 1998). ICA separates various sources of the fMRI signal by maximizing both the statistical independence and the non-Gaussianity of the source signals (McKeown et al., 1998; McKeown and Sejnowski, 1998; Hyvärinen, 1999, 2000). The capability of ICA to separate signal sources based on their non-Gaussian distributions could thus be used in differentiating nondeterministic physiological signal sources from fMRI data (Kiviniemi et al., 2000; Eke and Hermán, 1999; West et al., 1999; Obrig et al., 2000; McKeown et al., 1998; McKeown and Sejnowski, 1998).

In order to assess the analysis methods of spontaneous physiological fMRI signal sources, one should have strong nondeterministic signal sources and reduced artifacts in the data. Near infrared spectroscopy has shown that spontaneous background vasomotor fluctuations induce greater blood flow changes than neuronal activation during anesthesia (Kleinfeld et al., 1998). Under anesthesia, the very-low-frequency fluctuation (VLF) of 0.03 Hz actually dominates the fMRI signal in the primary functional regions (Kiviniemi et al., 2000). Anesthetized children usually have practically no motion artifacts. The circulatory system of child subjects is also stable compared to young adults based on the lower spectral power of heart rate variability (Pikku-jämsä et al., 1999). Thus, the anesthetized child brain seems like a stable model for analyzing the capability of ICA to separate nondeterministic physiological signal sources from brain fMRI data.

The aim in this study was to see whether ICA could separate the physiological signal sources of the brain. The hypothesis was that the statistically independent source signals are present in primary sensory cortices and that the sources are dominated by very-low-frequency fluctuation in the parenchyma. Also other physiological source signals, including CSF and blood flow pulsation, should be detectable. The spatial, frequency, and connectivity characteristics of statistically independent blood oxygen level dependent (BOLD) signal sources of resting state fMRI data during anesthesia were analyzed.

Materials and methods

Fifteen child subjects (7 females, 8 males, age range 2–9.5 years, mean 5.2) were imaged under thiopental anesthesia with an fMRI BOLD sequence after clinical brain imaging. The subject were recruited randomly in order of admittance. Midatzolam premedication (0.3 mg/kg) was given 2–3 h before the iv anesthesia with thiopental (average dose 6 mg/kg/h). The attending anesthesiologist sedated the subject into a state without voluntary motion while spontaneous breathing was ensured (Kiviniemi et al., 2000). The fMRI sequence was imaged, depending on the clinical MR, approximately 20–40 min from the onset of anesthesia. The Ethical Committee of Oulu University Hospital

approved the study and informed consent to the MRI scanning under anesthesia was obtained from the parents before clinical imaging.

The imaging was performed using a 1.5-T GE Signa MRI scanner (GE Medical Systems, Waukesha, WI, USA) with a birdcage head coil (Medical Advances, Milwaukee, WI, USA). In order to localize the region of interest for fMRI, several contiguous spin echo T1 weighted images were obtained in the sagittal plane using the following imaging parameters: TR = 400 ms, TE = 9 ms, matrix = 256^2. The fMRI study was performed based on a midline sagittal localizer. No stimulus was given to the subjects. Oblique axial slices covering an area from the lower edge of the cerebrum toward the parietal precentral gyrus were chosen in order to avoid susceptibility artifacts near the frontal and sphenoid sinuses. A 2.8 min time series of gradient echo EPI images of 7-mm thickness with a 5-mm interslice spacing was obtained. The other sequence parameters were TR = 2000 ms, TE = 40 ms, flip angle = 90°, matrix = 128^2. The 7-mm slice thickness was chosen in order to cover as large a volume of the brain as possible with the six slices with adequate signal-to-noise ratio. The standard automated shimming provided by the manufacturer was performed before each BOLD sequence. In order to keep the anesthetic procedure as short as possible, manual shimming could not be used. The motion of the head was further minimized with pillows. Hearing protection ear pads were used for protecting the ears from loud auditory activation.

Center of mass (COM) analysis of the imaged volume was used to detect the movement of the calculated center point of the brain in three (x, y, z) planes (Kiviniemi et al., 2000; Moser et al., 1996). None of the cases presented motion amplitude greater than 1 mm (max. motion 0.38 +/− 0.2 mm) threshold on the COM analysis. The first three images of the fMRI data set were left out of the analysis in order to obtain a signal at a dynamic steady state. Only voxels from within the brain were included in the analysis based on a previously used image signal intensity threshold (500) (Kiviniemi et al., 2000).

The overall spatial ICA analysis and voxel presentation were basically the same as those used by McKeown et al., with the exception of the ICA algorithm (McKeown et al., 1998; Hyvärinen, 1999, 2000). Here the ICA was done with FastICA, a freely available software tool developed using the MATLAB programming environment (Hyvärinen, 1999). FastICA is a faster and more robust algorithm than its predecessors (Hyvärinen, 1999). FastICA is based on the equivalence of finding maximally independent sources and finding sources whose distributions are as far from normal as possible, i.e., maximally non-Gaussian. We can measure the non-Gaussianity of a standardized random variable x by comparing the expectation of a suitable nonquadratic function G of x and the expectation of G for a standardized Gaussian random variable n as $[E\{G(x)\} - E\{G(n)\}]^2$. Here, E denotes the expectation operator or, in practice, the

average over the spatial distribution of a candidate source signal. FastICA searches over the space of different linear combinations of the brain images to find the local maxima of this non-Gaussianity measure, using a special fixed-point algorithm. The algorithm uses a nonlinearity function g that is the first derivative of the nonquadratic function G. FastICA reduces the dimension of the data with principal component analysis (PCA) as a preprocessing step. In this study the number of principal components was chosen to be 40 in order to cover at least 99.99% of the signal variance. The desired 40 independent components were calculated from the principal components with the default FastICA parameters (Approach:deflation, stabilization: off), with the exception of the nonlinearity function $g = $ tanh (Hyvärinen, 1999). The resulting independent components were then transformed into z-scores. Voxels that presented a z-score value of at least 6 were presented in spatial localization maps in green. In this article, the ICA component localization maps are referred to as ICA signal source maps.

From the initial 40 ICA component localization maps (i.e., 40 × 6 maps), those source maps containing clustered voxel groups in the functional brain areas and those related to major blood vessels and/or perivascular areas were chosen visually by the first author (VK). The criterion for the selection of a single parenchyma source map for further analysis was that the map should show a cluster of voxels on primary sensory cortex at the specific gyri without a wide spread of voxels. For the blood vessel related source maps, the selection criterion was the clustering of the detected voxels presenting fast pulsation in BOLD signal on the route of the middle, anterior, and posterior cerebral arteries simultaneously. The selectable signal sources in each functional or vascular area were calculated in order to evaluate the number of identifiable independent signal sources in the fMRI data. The anatomical spread and clustering were also qualitatively assessed.

The largest contiguous visual, auditory, sensorimotor, and blood vessel related ICA signal sources were further analyzed with regard to frequency characteristics. The frequency analysis was based on fast Fourier transformation (FFT) of the voxel time series of the ICA source maps. A mean FFT power spectral plot of all the image voxel data (total) was performed. Also the largest contiguous signal source of each functional area and a single blood vessel source was analyzed with FFT. The baseline noise power is known to follow a $1/f$ curve (Weisskoff et al., 1996). A baseline power curve was fitted into each FFT spectrum in the form

$$I(f) = a + bf^{-1}, \qquad (1)$$

where f represents the signal frequency, and I stands for spectral intensity (Kiviniemi et al., 2000). The unknown parameters a and b were estimated by manually fitting the baseline curve with a least-square error estimate; see also Fig. 4.

For the evaluation of the connectivity of the detected voxels, the mean intervoxel correlation coefficient (MCC) was calculated on a voxel by voxel basis,

$$\mathrm{MCC} = \frac{2}{n(n-1)} \sum_{i=1}^{n-1} \sum_{j=i+1}^{n} \mathrm{cc}_{ij}, \qquad (2)$$

where cc_{ij} is the correlation coefficient between the ith and the jth time course of the detected ICA map voxels. When a time course is being correlated with itself, i.e., $i = j$, the cc_{ij} was not used in the analysis. n refers to the number of detected voxels presenting fluctuation in the detected ICA component.

Results

Spatial distribution

ICA separated large and clustered individual signal sources in the visual cortex in each subject, as shown in Fig. 1. ICA was able to differentiate at least two sources in the visual areas in each case, three sources in 10 cases and four in 3 cases. Multiple signal sources of one example subject are shown in the upper row of Fig. 2. One case showed a source which followed the anatomy of the posterior cerebral artery as the most prominent in the visual cortex. In the rest of the subjects the selected sources followed dominantly the gyri of the parenchyma.

On average 1.85 independent signal sources were located at or near the auditory cortex in all of the subjects. Motor and sensory related signal sources could be located in 13 subjects with the average number of 2 and 1.53, respectively. The remaining 2 had no clearly detectable maps in the precentral or postcentral gyri. An example of a single subject is shown in Fig. 2 presenting the largest contiguous signal sources detected in each of the functional parenchyma.

Fig. 1. One ICA signal source map of the visual cortex of each of the subjects. The green color is overlaid on those voxels that exceed z-score 6 threshold. In some subjects, the source voxels are mixed with parts of the blood vessels, which may be due to partial voluming. Although there is interindividual variance, ICA was still able to separate multiple sources of the same kind in each subject.

Fig. 2. Multiple signal source maps of a single subject. ICA source signal maps present independent signal changes in the (A) central visual cortex and (B) associative visual areas. (C) Parts of the posterior cerebral blood vessels in the visual cortex depicted as a source of its own. (D) Signal source of auditory cortex. (E) Parts of the middle, anterior, and posterior cerebral artery (possibly in part with their perivascular spaces) which were presented as a signal source of their own in a similar manner for each subject. Notice that posterior cerebral arteries are separated as a unique source shown in C. (F) Spontaneous signal sources at the sensorimotor cortices.

3

4
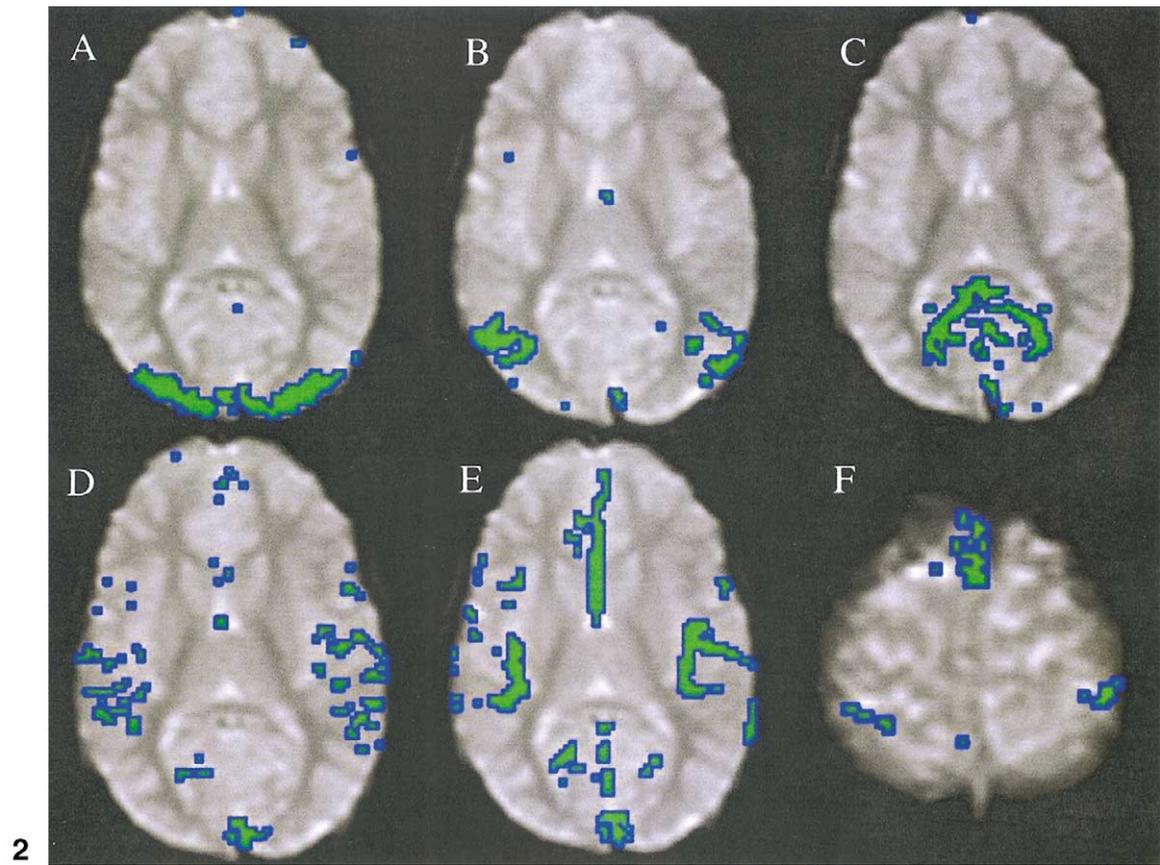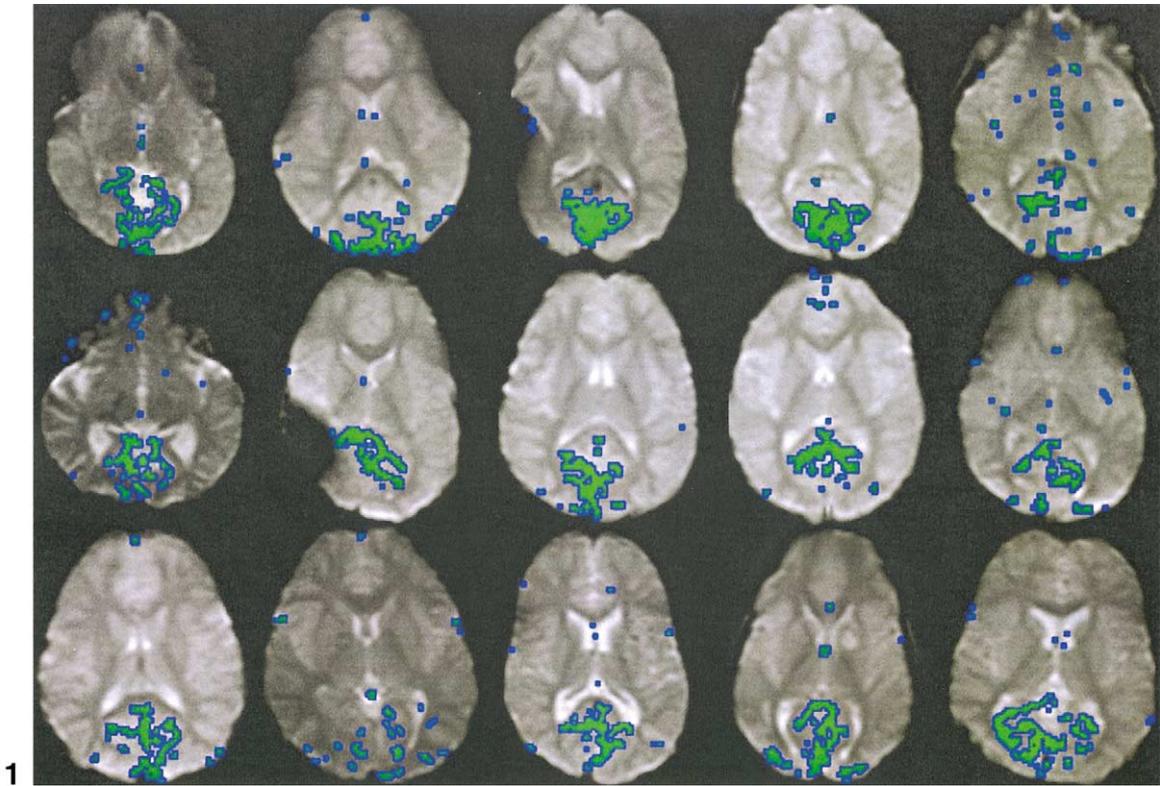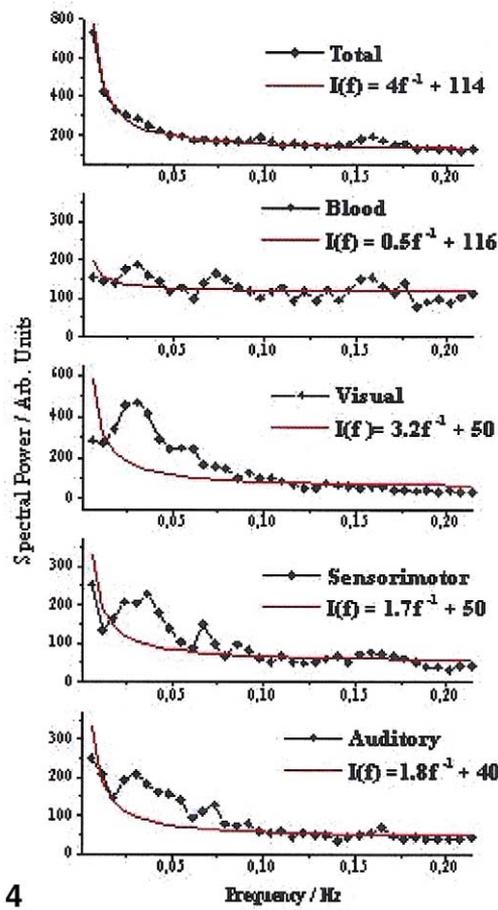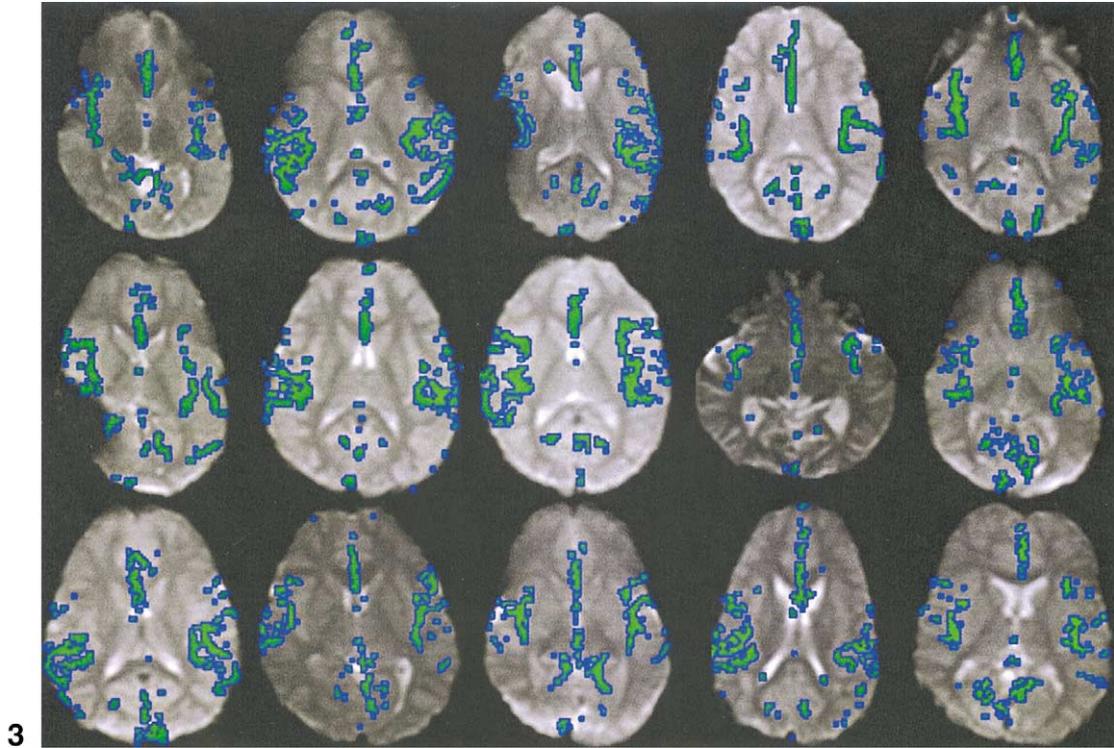
Major blood vessel areas and their perivascular spaces were shown to have a signal source of their own. At least two sources in different slices could be related to major arteries and one source map to the sagittal sinus in each case. The perivascular space cannot be separated from the blood vessels in these maps at the accuracy of this study, however. One signal source following the anatomy of a major blood vessel in the brain in each case can be seen in Fig. 3. Various other sources were detected in the brain, some resembling spatial distributions of random noise, motion artifacts, or CSF space pulsation. These were not further analyzed in this study. Qualitatively, the nonidentified signal sources were variable, sometimes clustered, but mostly the sources were not clearly defined into a single activation related area.

Frequency

The total image FFT spectrum of all the subjects revealed three power peaks over baseline noise and a $1/f$ distribution of frequencies (Fig. 4). The peaks were at 0.03, 0.1, and 0.152 Hz. Here parameter a was 110 and the b value was 4; c.f., the fitted curve in Fig. 4. This was in good agreement with our previous results (Kiviniemi et al., 2000).

The average FFT power spectral plot of the biggest signal source of the functional cortices is presented in the power spectra of Fig. 4. The average FFT power spectra of the signal sources of the functional parenchyma was clearly different from the average total image spectrum. Only the VLF fluctuation at 0.03 Hz had a dominant peak in all of the power spectra of the parenchyma. The visual $1/f$ baseline curve parameter a was estimated to be 50 and b 3.2. The baseline a values did not change significantly between the different cortices, but the curvature parameter b was smaller in the auditory (1.8) and sensorimotor areas (1.7) compared to the visual cortex. The parameters did not fit to the data due to the dominance of VLF and so the baseline curve does not seem to be exactly $1/f$.

The major blood flow related sources showed a less steep $1/f$ curve and more power peaks were present in the higher frequencies. The blood vessel power peaks are at 0.03, 0.73, and 0.152 Hz, resembling somewhat the total image spectra. The overall background intensity level a was 116 and b 0.5, which are different from the parenchyma signal sources (Fig. 4).

Connectivity

The connectivity of the detected voxels proved to be variable between source areas. The selected ICA signal source of the visual area had an average intervoxel MCC value of 0.29 (STD 0.09). The connectivity in the visual areas seems to be higher compared to other source signals of functional cortices. The MCC of sensorimotor and auditory signal sources were 0.17 (STD 0.09) and 0.15 (STD 0.065), respectively. The average MCC of the blood vessel related signal source maps was 0.26 (STD 0.14).

Discussion

The ICA was able to separate spatially independent signal sources related to nondeterministic physiological fluctuations in the anesthetized brain. On average, nine clustered signal sources could be identified in each subject at the functional cortices that are known to present dominant vasomotor fluctuation under an anesthetized condition (Kiviniemi et al., 2000; Kleinfeld et al., 1998). The signal sources closely resemble fMRI activation maps of primary and associative sensory and motor areas. ICA was able to separate several sources within the same functional areas in all subjects. In our experience, so many neuroanatomically accurate voxel clusters cannot be localized with time or frequency domain analysis methods from nonactivated fMRI data (Kiviniemi et al., 2000). Studies of anatomical overlap with fMRI activation results could not be obtained because of the unavoidable prolongation of anesthesia. The neurophysiological difference between the multiple statistically independent source signals in the same functional area remains to be determined.

The finding of three to four interindividually repeatable vascular signal sources in each case was a surprise, even though the pulsating blood flow is a probable signal source in the data. The spatial distribution of the blood vessel sources follows the routes of major branches of the anterior, middle, and posterior cerebral artery (Fig. 3). The multiple FFT power peaks of the blood vessel signal source suggest that the origin of signal variation is related to heart and respiratory pulsations (Fig. 4). The pulsatile blood flow changes may be reflected in the perivascular spaces and so they too may be involved in these signal sources. Despite

Fig. 3. Vascular ICA source maps for each subject detecting independent signal behavior in the major branches and/or perivascular Virchow spaces of the middle, anterior, and posterior cerebral artery. There seemed to be less overlap with the adjacent cortex in these sources. Only one such source is to be found in any one slice, and on average there are two in the whole image. A sagittal sinus source was also present in the most cranial slices of each subject, but they are not presented here.

Fig. 4. The average FFT power spectra. The fitted baseline power spectra curve [1] is shown in red with parameters a and b and the measured FFT power spectrum is shown in black. The total image power (Total) spectrum is shown at the top. Note the three peaks at 0.03, 0.1, and 0.152 Hz related to metabolic, myogenic, and respiratory fluctuation, respectively. The average FFT power spectrum of the blood vessel (Blood) signal sources from Fig. 3 is presented. The frequency distribution is similar to the total image spectrum, the power curve more linear, the peaks are low, and the baseline is elevated compared to the parenchyma signal sources. Overall the baseline parameter a did not change that much but the constant b showed clear differences between spectra. The visual (Visual), sensorimotor (Sensorimotor), and auditory (Auditory) signal source FFT power spectra present a clear elevation in the VLF frequencies (0.03 Hz), whereas the higher frequencies have relatively low power.

the clear anatomical resemblance to arterious and venous structures, further angiographic correlation of the blood vessel signal sources is needed. The interindividual consistency of the vascular sources suggests that the FastICA is quite reproducible in its ability to localize physiological BOLD signal sources (Fig. 3).

Fig. 4 shows that the 0.03 Hz fluctuation is a dominant frequency above the baseline in the total image, blood vessels, and in each functional parenchyma. The finding of parenchyma sources matches previous findings on functional cortex BOLD signal fluctuations (Biswal et al., 1995; Cordes et al., 2000, 2001; Kiviniemi et al., 2000; Kleinfeld et al., 1998). The origin of VLF fluctuation may be related to vasomotion since the same frequency is prominent in the blood vessels and in the total image as well. On the other hand, the total image and blood vessel spectra have peaks in higher frequencies that are not present in the cortical sources (Fig. 4). The two different fluctuation frequencies (0.03 and 0.1 Hz) may be related to different types blood flow control, i.e., metabolic and myogenic, respectively (Panerai et al., 1998; Obrig et al., 2000; Zhang et al., 2000; Wagner and Persson, 1994). Based on the power spectral results of this study, it can be hypothesized that a difference in blood flow control exists between the arteries and cortical capillaries in anesthesia.

The *a* and *b* parameters differed in the source signals compared to the total image spectrum. The functional signal sources have a reduced baseline power value *a* compared to the total image and blood vessels (Fig. 3). The curvature parameter *b* shows a clear difference between the cortical and blood vessel sources. The changes in the parameters indicate that signal variations of physiological signal sources can be evaluated on the overall appearance of the power spectra and not only on one single frequency peak (Fig. 4). The difficulties in fitting parameters *a* and *b* to the data suggest that cortical signal sources follow a baseline frequency power distribution of $I(f) = a + bf^{-\alpha}$, where $\alpha \neq 1$. Studies on volunteers point out that the α does change due to elevation of low-frequency fluctuation that follows sedation (Kiviniemi et al., 2002).

The connectivity characteristics were used for comparison on an average level with the previously detected COSLOFF indices (Li et al., 1999). The MCC parameter presented here is not strictly identical to COSLOFF, but they give the same kind of results. MCC correlates each voxel time course with all others and COSLOFF uses a single, selected reference time course in the analysis. Compared to COSLOFF measurements of hippocampus connectivity in normal volunteers, the MCC of the most prominent source signal in the visual cortex is almost identical, i.e., COSLOFF = 0.3 vs MCC = 0.29. The connectivity of the other functional sources seems to be lower compared to the visual signal sources, which is not easily explained. In this study, the selected functional sources were dominated by a 0.03-Hz fluctuation, which is in good agreement with the finding that a major part of the connectivity is related to signal frequencies under 0.1 Hz (Cordes et al., 2001).

A problem with ICA is that it gives a large number of components with no particular order, which means that a given physiological signal source could be expressed in any one of the 40 ICA components. Comparison of repetitive ICA analysis of the same data is complicated for the same reason, and subjective decision-making cannot be avoided. Topographical and frequency-based ordering of the components has recently been proposed and may prove important in further use of ICA (Hyvärinen, 2001; Moritz et al., 2001). One problem is the similarity and overlap of some of the source signals and other components. Focusing on the known anatomical areas that present vasomotor or blood flow related signal sources was used as a selection criterion between the components in this article. The PCA preprocessing step of the FastICA is conducted primarily as a method of noise reduction, but there is also a possibility of losing subtle source signal information. After PCA reduction of the matrix to 40 components, however, the ICA source maps can still explain over 99.99% of the signal variance.

The correct interpretations of the findings are challenging due to the aliasing of faster respiratory and cardiac pulsation to the rather undersampled fMRI data (Frank et al., 2001). If the dominant VLF fluctuation was a product of aliasing it should change when the TR is changed. In this study, the TR was 2 s instead of the 3 s that was used in our previous study. However, the dominant VLF peak of the functional parenchyma BOLD signal spectral power is at the same 0.03-Hz frequency in both studies (Kiviniemi et al., 2000). So aliasing of faster physiological events does not necessarily explain all signal changes of the VLF range. Some of the subjects had extracranial metal implants including drainage shunts inducing susceptibility artifacts. Nyqvist ghosting was seen in some of the cases (Figs. 1–3). It would be interesting to image anesthetized subjects with subsecond TRs, navigator based head motion detection, and slab shimming to see whether these procedures change the results obtained here. There is no doubt that the various pathological conditions influence the source signals of the child subjects, and thus the ICA sources should be correlated with normal awake controls. Despite all the shortcomings of our data the FastICA succeeds in separating statistically independent signal sources in areas known to exhibit dominant physiological changes with interindividual consistency (Figs. 1 and 3).

Frequency domain power encoding detects signals that contain a fixed frequency without frequency or phase variance. With time domain methods one must either identify or estimate the physiological signal among voxel time-courses, even though one cannot predict their nature. The blood flow changes in the brain cortex that influence the fMRI signal are nondeterministically stochastic and non-Gaussian in distribution during rest (Coca et al., 1998; Frank et al., 2001; Eke and Hermán, 1999; Rossitti and Stephensen, 1994).

With spatial domain ICA the basic neurophysiological assumption is that one empirically knows where to look for fMRI source signals. Compared to manual segmentation of voxels, the advantage of ICA is essentially the statistical independence of the detected voxels in a segmented ICA source. The dual nature of statistical analysis of independence and signal source based segmentation of the voxels for further analysis makes the spatial domain ICA a versatile method for assessing stochastic physiological signals in fMRI data.

Conclusion

ICA can separate multiple, statistically independent, physiological signal sources in the primary sensory areas and major blood vessels in anesthetized brain fMRI. The spatial and frequency characteristics of the functional signal sources match with the previous knowledge of vasomotor waves in the functional parenchyma during anesthesia. ICA exceeds the capability of previously used frequency and time domain methods in physiological source signal localization. The ICA is a potential tool for assessing statistical independence and for segmenting neurophysiological source signals for further analysis. The advantage of ICA is that it is a data-driven, distribution-based method which is suitable for analyzing nondeterministic signal sources such as resting state vasomotor fluctuations or blood vessel pulsations.

References

Biswal, B.B., Yetkin, F.Z., Haughton, V.M., Hyde, J.S., 1995. Functional connectivity in the motor cortex of resting human brain using echo-planar MRI. Magn. Reson. Med. 34, 537–541.

Coca, D., Zheng, Y., Mayhew, J.E.W., Billings, S.A., 1998. Non-linear analysis os vasomotion oscillations in reflected light measurements, in: Oxygen Transport to Tissue XX, Plenum, New York, pp. 571–582.

Cordes, D., Haughton, V.M., Arfanakis, K., Wendt, G.J., Turski, P.A., Moritz, C.H., Quigley, M.A., Meyerand, M.E., 2000. Mapping functionally related regions of brain with functional connectivity MR imaging. Am. J. Neur. Rad. 21, 1636–1644.

Cordes, D., Haughton, V.M., Arfanakis, K., Carew, J.D., Turski, P.A., Moritz, C.H., Quigley, M.A., Meyerand, M.E., 2001. Frequencies contribution to functional connectivity in the cerebral cortex in "resting-state" data. Am. J. Neur. Rad. 22, 1326–1333.

Eke, A., Hermán, P., 1999. Fractal analysis of spontaneous fluctuations in human cerebral hemoglobin content and its oxygenation level recorded by NIRS, in: Oxygen Transport to Tissue XXI, Plenum, New York, pp. 49–55.

Frank, L., Buxton, R., Wong, E., 2001. Estimation of respiration-induced noise fluctuations from undersampled multislice fMRI data. Magn. Reson. Med. 45, 635–664.

Hyvärinen, A., 1999. Fast and robust fixed-point algorithms for independent component analysis, IEEE. Trans. Neural Netw. 10 (3), 626–634.

Hyvärinen, A., Hoyer, P.O., Inki, M., 2001. Topographic independent component analysis. Neural Comput. 13 (7), 1527–1558.

Hyvärinen, A., Oja, E., 2000. Independent component analysis: algorithms and applications. Neural Netw. 13 (4–5), 411–430.

Kiviniemi, V., Jauhiainen, J., Tervonen, O., Pääkkö, E., Oikarinen, J., Vainionpää, V., Rantala, H., Biswal, B., 2000. Slow vasomotor fluctuation in the fMRI of the anesthetized child brain. Magn. Reson. Med. 44, 378–383.

Kiviniemi, V., Haanpää, H., Kantola, J., Alahuhta, S., Vainionpää, V., Jauhiainen, J., Tervonen, O., 2002. The effect of midazolam sedation on baseline fMRI signal. MAGMA 15 (Suppl. 1), 116 (abstract 246).

Kleinfeld, D., Mitra, P.P., Helmchen, F., Denk, W., 1998. Fluctuations and stim+ulus-induced changes in blood flow observed in individual capillaries in layers 2 through 4 of rat neocortex. Proc. Natl. Acad. Sci. USA 95 (26), 15741–15746.

Li, Z., Li, S-J., Biswal, B.B., Antuono, P., Jones, J., 1999. Functional connectivity in hippocampal region of Alzheimer's subjects, in: Proceedings of the ISMRM, 7th Annual Meeting, Philadelphia, p. 817.

McKeown, M.J., Makeig, S., Brown, G.B., Jung, T-B., Kindermann, S.S., Bell, A.J., Sejnowski, T.J., 1998. Analysis of fMRI data by blind source separation into independent spatial components. Hum. Brain Mapping 6, 160–188.

McKeown, M.J., Sejnowski, T.J., 1998. Independent component analysis of fMRI data: examining the assumptions. Hum. Brain Mapping 6, 368–372.

Mitra, P.P., Ogawa, S., Hu, X., Ugurbil, K., 1997. The nature of spatio-temporal changes in cerebral hemodynamics as manifested in functional magnetic resonance imaging. Magn. Reson. Med. 37, 551–518.

Moritz, C., Carew, J.D., Haughton, V.M., Meyerand, M.E., 2001. Frequency domain ranking independent component analysis of a fMRI complex motor paradigm, Proc. Joint Ann. Meet. ISMRM ESMRMB, Glasgow (abstract 1726).

Moser, E., Teichtmeister, C., Diemling, M., 1996. Reproducibility and postprocessing of gradient-echo functional MRI to improve localization of brain activity in the human visual cortex. Magn. Reson. Imag. 14 (6), 567–579.

Obrig, H., Neufang, M., Wenzel, R., Kohl, M., Steinbrink, J., Einhäupl, K., Villringer, A., 2000. Spontaneous low frequency oscillations of cerebral hemodynamics and metabolism in human adults. NeuroImage 12, 623–639, doi:10.1006/nimg.2000.0657.

Ogawa, S., Lee, T.M., Kay, A.R., Tank, D.W., 1990. Brain magnetic resonance imaging with contrast dependent on blood oxygenation. Proc. Natl. Acad. Sci. USA 87 (24), 9868–9872.

Ogawa, S., Menon, R.S., Kim, S.G., Ugurbil, K., 1998. On the characteristics of functional magnetic resonance imaging of the brain. Ann. Rev. Biophys. Biomol. Struct. 27, 447–474.

Oppenheim, A.V., Willsky, A.S., Nawab, S.H., 1996. Signals and Systems, second ed. Prentice Hall, Upper Saddle River, NJ.

Panerai, R.B., Rennie, J.M., Kelsall, A.W.R., Evans, D.H., 1998. Frequency-domain analysis of cerebral autoregulation from spontaneous fluctuations in arterial pressure. Med. Biol. Eng. Comput. 36, 315–322.

Pikkujämsä, S.M., Mäkikallio, T.H., Sourander, L.B., Räihä, I.J., Puukka, P., Skytta, J., Peng, C.K., Goldberger, A.L., Huikuri, H.V., 1999. Cardiac interbeat dynamics from childhood to senescence: comparison of conventional and new measures based on fractals and chaos theory. Circulation 100 (4), 393–399.

Rossitti, S., Stephensen, H., 1994. Temporal heterogeneity of the blood flow velocity at the middle cerebral artery in normal human characterized by fractal analysis. Acta Physiol. Scand. 151, 191–198.

Wagner, C.D., Persson, P.B., 1994. Two ranges in blood pressure power spectrum with different $1/f$ characteristics. Am. J. Physiol. 267, H449–H454.

Weisskoff, R.M., Baker, J., Belliveau, J., 1996. Power spectrum analysis of functionally-weighted MR data: what's in the noise? Proc. 12th SMRM, New York, p. 7.

West, B.J., Zhang, R., Sanders, A.W., Miniyar, S., Zuckerman, J.H., Levine, B.D., 1999. Fractal fluctuations in transcranial Doppler signals. Phys. Rev. E 59 (3), 3492–3498.

Zhang, R., Zuckerman, J.H., Levine, B.D., 2000. Spontaneous fluctuations in cerebral blood flow: insight from extended recordings in humans. Am. J. Physiol. 278, H1848–H1855.